# In-flight Actuator Failure Recovery of a Hexrotor via Multiple Models and Extended High-Gain Observers

Connor J. Boss<sup>1</sup> and Vaibhav Srivastava<sup>1</sup>

Abstract—We study an in-flight actuator failure recovery problem for a hexrotor UAV. The hexrotor may experience external disturbances and modeling error, which are accounted for in the control design and distinguished from an actuator failure. A failure of any one actuator occurs during flight and must be identified quickly and accurately. This is achieved through the use of a multiple-model, multiple extended high-gain observer (EHGO) based output feedback control strategy. The family of EHGOs are responsible for estimating states, disturbances, and are used to select the appropriate model based on the system dynamics after a failure has occurred. The proposed method is theoretically analyzed and validated through simulations and experiments.

**Index Terms**—Failure Detection and Recovery, Aerial Systems: Mechanics and Control

#### I. Introduction

ITH increased dependence on multi-rotor UAVs in many mission critical applications from infrastructure inspection to aerial cinematography to reconnaissance and surveillance, the demand for increasingly reliable vehicles is growing. In these applications, the loss of a vehicle poses significant threats to financial, security, or personnel interests. Improvements in control strategies as well as improvements in both software and hardware implementation have increased reliability greatly. However, there is still significant room for improvement in the face of actuator failures.

Actuator failure is of particular interest when it comes to reliability, as conventional multi-rotor UAVs will crash, or at least require an emergency landing, in the event of a failure. The main challenges in recovering from an actuator failure during flight are the ability to quickly detect the failure and to reconfigure the system while preserving stability. A complete actuator failure will cause a large rotational torque, which in turn causes the UAV to roll and pitch rapidly. If action is not taken extremely quickly the UAV can arrive at a configuration where it simply cannot recover.

The area of fault detection and isolation has been investigated for generalized systems [1-4], as well as for multi-

Manuscript received: February 7, 2021; Revised May 5, 2021; Accepted June 9, 2021.

This paper was recommended for publication by Editor Clement Gosselin upon evaluation of the Associate Editor and Reviewers' comments. This work has been supported in part by NSF Award IIS-1734272 and NASA MSGC Award 80NSSC20M0124.

<sup>1</sup>C. J. Boss and V. Srivastava are with The Department of Electrical and Computer Engineering, Michigan State University, East Lansing, MI, 48823 USA {bossconn, vaibhav}@egr.msu.edu

Digital Object Identifier (DOI): see top of this page.

rotor UAVs, including quadrotors [5–9], hexrotors [10–13], and octorotors [14, 15]. A quadrotor with failure of one actuator or two opposing actuators can be stabilized, but loses yaw controllability [5]. A failure on an octorotor can result in dramatically reduced thrust capability [14, 15]. Interestingly, a standard hexrotor is fully vulnerable to any single actuator failure because the total moment generated by opposed rotors are collinear [16], resulting in an uncontrollable system.

In order to overcome this vulnerability, a variety of modifications have been proposed. One option is to use a different pattern of rotor rotation directions [10, 12], thus making the moment of certain pairs of opposed rotors non-collinear. This will maintain controllability under failure, however, the asymmetry restricts this method to only recover if one of four specific rotors fail. Another option [13, 16] involves a modified airframe design where the actuators are canted off plane to enable force application in all six degrees of freedom. This method supports the loss of any one actuator, however, given the orientation of the rotors, the configuration is not efficient for nominal flight. A third option is to enable the rotors to rotate in either direction [11]. This method maintains controllability if any one of the actuators fail, while preserving efficiency during nominal flight. Thus, we will utilize this hardware reconfiguration strategy as well.

The detection strategies used in the methods described above include a linear observer [12], estimating actuator forces using a sliding-mode differentiator on IMU data [9], and an Extended Kalman Filter based rotor health estimator [11], while others have left the detection strategy to future work [5, 14, 15]. In contrast, we utilize a multiple-model multiple EHGO output feedback linearizing control approach, in which estimates from the EHGOs are used to detect and classify a failure. The EHGOs not only allow us to detect failures and select the appropriate reconfiguration, but are fully integrated in our control strategy to provide estimates of unmeasured states and disturbances. These estimates are used before, during, and after failure, to improve tracking performance in the presence of a broad class of disturbances.

While disturbance observers have been used in multi-rotor control [17, 18], EHGOs are not typically implemented on highly dynamic systems of this nature due to high sample rate requirements and possible measurement noise amplification. This work serves to show that even at a relatively low sample rate of 100Hz, EHGOs can be implemented on highly dynamic systems in practice. Furthermore, EHGOs afford the ability to estimate and cancel a broader class of disturbances than

standard disturbance observers [19].

The failure recovery methods described thus far do not consider disturbances affecting the system. Our method explicitly incorporates disturbances and can differentiate between disturbances and an actuator failure, depending on disturbance levels. The analysis presented here not only guarantees stability, but provides insights into what levels of disturbances can be distinguished from an actuator failure and how much time can elapse between failure and switching models before risking losing control. Finally, we illustrate the effectiveness of our approach through simulation and experimental results.

The paper is organized as follows. The system dynamics are in Section II, and the control law is designed in Section III. The failure recovery strategy is in Section IV, with stability analysis in Section V. Simulation and experimental results are presented in Section VI and Section VII, respectively, with conclusions in Section VIII.

#### II. SYSTEM DYNAMICS

A hexrotor UAV dynamics are split into two subsystems: the rotational dynamics and the translational dynamics.

#### A. Rotational Dynamics

Let  $\theta_1 = [\phi \ \theta \ \psi]^\top \in (-\frac{\pi}{2}, \frac{\pi}{2})^2 \times (-\pi, \pi]$  be the Euler angles describing the hexrotor orientation in the inertial frame, and let  $\theta_2 = [\dot{\phi} \ \dot{\theta} \ \dot{\psi}]^\top \in \mathbb{R}^3$  be the associated angular rates. Let  $\theta_r = [\phi_r \ \theta_r \ \psi_r]^\top \in (-\frac{\pi}{2}, \frac{\pi}{2})^2 \times (-\pi, \pi]$  and  $\dot{\theta}_r = [\dot{\phi}_r \ \dot{\theta}_r \ \dot{\psi}_r]^\top \in \mathbb{R}^3$  be the rotational reference signals. Define the rotational tracking error,  $\boldsymbol{\xi}$ , by

$$\boldsymbol{\xi}_1 = \boldsymbol{\theta}_1 - \boldsymbol{\theta}_r, \quad \boldsymbol{\xi}_2 = \dot{\boldsymbol{\xi}}_1 = \boldsymbol{\theta}_2 - \dot{\boldsymbol{\theta}}_r, \quad \boldsymbol{\xi} = [\boldsymbol{\xi}_1^\top \ \boldsymbol{\xi}_2^\top]^\top.$$

Defining the inertia matrix,  $J \in \mathbb{R}^{3\times3}$ , a matrix  $\Psi \in \mathbb{R}^{3\times3}$  which transforms body-fixed angular velocity to Euler angular rates [20], and its associated derivative,  $\dot{\Psi} \in \mathbb{R}^{3\times3}$ , the rotational tracking error dynamics are

$$\dot{\boldsymbol{\xi}}_1 = \boldsymbol{\xi}_2, 
\dot{\boldsymbol{\xi}}_2 = f(\boldsymbol{\xi}, \boldsymbol{\theta}_1, \dot{\bar{\boldsymbol{\theta}}}_r) + G(\boldsymbol{\theta}_1)\boldsymbol{\tau} + \boldsymbol{\varsigma}_{\mathcal{E}}, \tag{1}$$

where

$$\begin{split} f(\xi,\theta_1,\dot{\bar{\theta}}_r) &= \dot{\Psi} \Psi^{-1}(\xi_2 + \dot{\bar{\theta}}_r) \\ &- \Psi J^{-1}(\Psi^{-1}(\xi_2 + \dot{\bar{\theta}}_r) \times J \Psi^{-1}(\xi_2 + \dot{\bar{\theta}}_r)), \\ G(\theta_1) &= \Psi J^{-1}, \end{split}$$

 $\dot{\boldsymbol{\theta}}_r$  is some approximation of  $\dot{\boldsymbol{\theta}}_r$ ,  $\boldsymbol{\tau} \in \mathbb{R}^3$  is a vector of body-fixed torques,  $\boldsymbol{\varsigma}_{\boldsymbol{\xi}} = \boldsymbol{\sigma}_{\boldsymbol{\xi}} - \ddot{\boldsymbol{\theta}}_r + [f(\boldsymbol{\xi}, \boldsymbol{\theta}_1, \dot{\boldsymbol{\theta}}_r) - f(\boldsymbol{\xi}, \boldsymbol{\theta}_1, \dot{\boldsymbol{\theta}}_r)] \in \mathbb{R}^3$  is an added term to represent the lumped rotational disturbance which satisfies *Assumption 1* (stated below), and  $\boldsymbol{\sigma}_{\boldsymbol{\xi}} \in \mathbb{R}^3$  is the nominal rotational disturbance term [20] in the original rotational dynamics with a generic control input.

Assumption 1 (Properties of Disturbances): For a control system with state  $x \in \mathbb{R}^n$ , expressed in lower triangular form, such as (1), any disturbance term is assumed to enter only the  $x_n$  dynamics. The disturbance term is also assumed to be continuously differentiable and its partial derivatives with respect to states are bounded on compact sets of those states for all  $t \ge 0$  [20].

## B. Translational Dynamics

Let  $p_1 = [x \ y \ z]^{\top} \in \mathbb{R}^3$  and  $p_2 = [\dot{x} \ \dot{y} \ \dot{z}]^{\top} \in \mathbb{R}^3$  be the position and velocity of the hexrotor center of mass. Let  $p_r = [x_r \ y_r \ z_r]^{\top} \in \mathbb{R}^3$  and  $\dot{p}_r = [\dot{x}_r \ \dot{y}_r \ \dot{z}_r]^{\top} \in \mathbb{R}^3$  be the translational reference signals. Define the translational tracking error,  $\rho$ , by

$$\rho_1 = \boldsymbol{p}_1 - \boldsymbol{p}_r, \quad \rho_2 = \dot{\boldsymbol{\rho}}_1 = \boldsymbol{p}_2 - \dot{\boldsymbol{p}}_r, \quad \boldsymbol{\rho} = [\boldsymbol{\rho}_1^\top \ \boldsymbol{\rho}_2^\top]^\top.$$

Taking the third column of the rotation matrix describing the hexrotor orientation in the inertial frame as  $R_3(\theta_1) \in \mathbb{R}^3$ , as in [20], g as the gravitational constant,  $u_f \in \mathbb{R}$  as the total thrust input,  $m \in \mathbb{R}_{>0}$  as the mass, and defining  $e_z = [0 \ 0 \ 1]^T$ , the translational tracking error dynamics are

$$\dot{\boldsymbol{\rho}}_1 = \boldsymbol{\rho}_2, \dot{\boldsymbol{\rho}}_2 = -\frac{u_f}{m} R_3(\boldsymbol{\theta}_1) + g \boldsymbol{e}_z + \boldsymbol{\sigma}_\rho - \ddot{\boldsymbol{p}}_r,$$
 (2)

where  $\sigma_{\rho} \in \mathbb{R}^3$  is an added term to represent the lumped translational disturbance which also satisfies *Assumption 1*.

# C. Failure Modes and Mapping Actuator Speeds to Inputs

We will now consider how the system inputs in the form of body-torques,  $\tau$ , and thrust force,  $u_f$ , are applied by the actuators, and how this changes during a failure.

Remark 1 (Bidirectional Rotor Rotation): Bidirectional rotors are a requirement for a model switching failure recovery based on the controllability of the system.

Since we require bidirectional rotor rotation, and the rotors are designed for efficient operation in only one direction, we define a pair of thrust coefficients,  $b^+ \in \mathbb{R}_{>0}$  for normal operation and  $b^- \in \mathbb{R}_{>0}$  for reverse operation. These coefficients relate rotor speed,  $\omega \in \mathbb{R}$ , to force,  $\bar{f} \in \mathbb{R}$ , as

$$\bar{f}_j = \begin{cases} b^+ \omega_j^2, & \text{for } \omega_j \ge 0, \\ -b^- \omega_j^2, & \text{for } \omega_j < 0, \end{cases} \quad \text{for } j \in \{1, \dots, 6\}. \quad (3)$$

Let  $i \in \{0, ..., 6\}$  denote failure modes such that i = 0 corresponds to no failure and  $i \neq 0$  corresponds to the failure of the i-th rotor. Let  $\mathcal{F}^{(i)} \in \mathbb{R}^{6 \times 6}$  be the failure matrix associated with failure mode i, defined by  $\mathcal{F}^{(0)} = I_6$  and

$$\mathcal{F}^{(i)} = \begin{bmatrix} d_1 \\ \ddots \\ d_6 \end{bmatrix}, \quad \text{with } d_j = \begin{cases} 0, & \text{for } j = i, \\ 1, & \text{otherwise,} \end{cases}$$
 (4)

for  $j \in \{1, ..., 6\}$ . Let  $M \in \mathbb{R}^{4 \times 6}$  be the mapping between actuator forces and system inputs and be defined by

$$M = \begin{bmatrix} \frac{1}{-\frac{r}{2}} & \frac{1}{-r} & \frac{1}{r} & \frac{1}{r} & \frac{1}{r} \\ \frac{r\sqrt{3}}{2} & 0 & -\frac{r\sqrt{3}}{2} & -\frac{r\sqrt{3}}{2} & 0 & \frac{r\sqrt{3}}{2} \\ 0 & -c & c & -c & c & -c \end{bmatrix},$$
 (5)

where  $r \in \mathbb{R}_{>0}$  is the distance from the hexrotor center of mass to the center of an actuator, and  $c \in \mathbb{R}_{>0}$  is the aerodynamic drag coefficient of a rotor. Let  $i_t^*$  be the true failure mode at time t,  $i_t$  be the failure mode that is selected at time t, and  $t_f$  be the time of failure.

$$\begin{bmatrix} u_f \\ \tau \end{bmatrix} = M\mathcal{B}\mathcal{F}^{(i_t)}\omega_s, \quad \mathcal{B} = \begin{bmatrix} v_1 b^{\nu_1} \\ & \ddots \\ & & v_c b^{\nu_6} \end{bmatrix}, \quad (6)$$

where  $v_i \in \{-, +\}$  is the sign of  $\omega_i$ .

Assumption 2 (Single Failure Occurrence): We assume  $i_t^* = i_t = 0$  for  $t < t_f$ . At the time of failure  $i_{t_f}^* = 0 \rightarrow i_t^* \in \{1, \dots, 6\}$  for  $t > t_f$ . Since our platform is a hexrotor, we focus on a single actuator failure to ensure the system retains full controllability. Failure of more than one actuator, in specific cases, can result in a system that retains controllability. However, in these configurations, only two of the actuators would be responsible for generating the total lifting thrust, with the others providing small correctional forces and torques. Consequently, due to limited actuator power, the hexrotor would not be able to maintain altitude.

### III. OUTPUT FEEDBACK CONTROL DESIGN

In this section, an output feedback estimation and control strategy is designed as in [20]. We utilize the same control and observer design, while extending our previous work to incorporate a family of EHGOs to estimate not only modeling error and external disturbances, but errors due to the failure of any one actuator, as well as enabling the detection of a failure through the use of the observer estimates. As such, each observer will correspond to a possible plant configuration, i.e., a nominal model and six failure models.

# A. Extended High-Gain Observer Design

A family of multi-input multi-output EHGOs is designed to estimate higher-order states of the error dynamic systems (1) and (2), and uncertainties arising from modeling error, external disturbances, and actuator failure [21]. It is shown in [20, 22] that it is necessary to include actuator dynamics in the multirotor model for EHGO design. For a desired rotor speed,  $\omega^{\text{des}}$ , the actuators can be modeled as a first-order system with time constant,  $\tau_m \in \mathbb{R}_{>0}$ , given by  $\tau_m \dot{\omega}_j = (\omega_j^{\text{des}} - \omega_j)$ , for  $j \in \{1, \ldots, 6\}$ . The actuator dynamics must be included in the EHGO because in practice  $\tau_m$  and  $\epsilon$  are of similar magnitude, so both reside in the same time-scale. These dynamics then form the input to the EHGO as in [20].

The rotational and translational tracking error dynamics are combined and the state-space is extended to estimate disturbance vectors for both subsystems. For the purposes of writing the observer under the *i*-th failure mode, we write the extended system dynamics in the following form

$$\dot{\rho}_{1} = \rho_{2}, 
\dot{\rho}_{2} = -\frac{u_{f}}{m} R_{3}(\theta_{1}) + g \boldsymbol{e}_{z} + \boldsymbol{\sigma}_{\rho} - \ddot{\boldsymbol{p}}_{r}, 
\dot{\boldsymbol{\sigma}}_{\rho} = \varphi_{\rho}(t, \boldsymbol{\rho}), 
\dot{\boldsymbol{\xi}}_{1} = \boldsymbol{\xi}_{2}, 
\dot{\boldsymbol{\xi}}_{2} = f(\boldsymbol{\xi}, \theta_{1}, \dot{\boldsymbol{\theta}}_{r}^{(i_{t})}) + \tilde{G}M\mathcal{B}\mathcal{F}^{(i)}\boldsymbol{\omega}_{s}^{(i_{t})} + \bar{\boldsymbol{\varsigma}}_{\xi}^{(i)}, 
\dot{\boldsymbol{\varsigma}}_{\xi}^{(i)} = \varphi_{\xi}^{(i)}(t, \bar{\boldsymbol{\varsigma}}_{\xi}^{(i)}),$$
(7)

where  $\bar{\boldsymbol{\varsigma}}_{\xi}^{(i)} = \boldsymbol{\sigma}_m^{(i)} + \boldsymbol{\varsigma}_{\xi}$ , and  $\boldsymbol{\sigma}_m^{(i)} = \tilde{\boldsymbol{G}} \boldsymbol{M} \boldsymbol{\mathcal{B}} (\boldsymbol{\mathcal{F}}^{(i_t^*)} - \boldsymbol{\mathcal{F}}^{(i)}) \boldsymbol{\omega}_s^{(i_t)}$  is the error resulting from an incorrect model,  $i_t \neq i_t^*$ . Finally,  $\tilde{\boldsymbol{G}} = [0_{3\times 1} \; \boldsymbol{G}(\boldsymbol{\theta}_1)]$  and  $\boldsymbol{\sigma}_m^{(i_t^*)} = 0$ . Here,  $\varphi_{\rho}(t, \boldsymbol{\rho})$  and  $\varphi_{\xi}^{(i)}(t, \bar{\boldsymbol{\varsigma}}_{\xi}^{(i)})$  are unknown functions describing the translational and rotational disturbance dynamics.

3

Assumption 3 (Disturbance Dynamics): It is assumed that  $\varphi_{\rho}(t, \rho)$  and  $\varphi_{\xi}^{(i)}(t, \bar{\varsigma}_{\xi}^{(i)})$  are continuous and bounded on any compact set in the domain of  $\rho$  and  $\bar{\varsigma}_{\xi}^{(i)}$ , respectively.

compact set in the domain of  $\rho$  and  $\bar{\varsigma}_{\xi}^{(i)}$ , respectively. The observer system is written with extended states and directional squared rotor speeds as the input,  $\omega_s^{(i_t)}$ . Defining the following state vectors

$$\chi_1 = [\boldsymbol{\rho}_1^\top \ \boldsymbol{\rho}_2^\top \ \boldsymbol{\sigma}_{\rho}^\top]^\top, \quad \chi_2 = [\boldsymbol{\xi}_1^\top \ \boldsymbol{\xi}_2^\top \ \boldsymbol{\zeta}_{\xi}^\top]^\top, \quad \chi = [\boldsymbol{\chi}_1^\top \ \boldsymbol{\chi}_2^\top]^\top,$$
we can write the EHGOs in a compact form as
$$\dot{\hat{\chi}}^{(i)} = A\hat{\chi}^{(i)} + B\left[\bar{f}(\hat{\chi}^{(i)}, \boldsymbol{\theta}_1, \dot{\bar{\boldsymbol{\theta}}}_r^{(i_t)}) + \bar{G}^{(i)}(\boldsymbol{\theta}_1)\boldsymbol{\omega}_s^{(i_t)}\right] + H\hat{\chi}_e^{(i)},$$

$$\hat{\chi}_e^{(i)} = C(\chi - \hat{\chi}^{(i)}),$$

where  $\hat{\chi}^{(i)} = \left[\hat{\rho}_1^{(i)\top} \hat{\rho}_2^{(i)\top} \hat{\sigma}_{\rho}^{(i)\top} \hat{\xi}_1^{(i)\top} \hat{\xi}_2^{(i)\top} \hat{\xi}_{\xi}^{(i)\top}\right]^{\top}$  is the estimate of  $\chi$  under the model with failure i, and

$$\begin{split} A &= \oplus_{j=1}^2 A_j, \ B = \oplus_{j=1}^2 B_j, \ C = \oplus_{j=1}^2 C_j, \ H = \oplus_{j=1}^2 H_j, \\ A_j &= \begin{bmatrix} 0_3 & I_3 & 0_3 \\ 0_3 & 0_3 & I_3 \\ 0_3 & 0_3 & 0_3 \end{bmatrix}, \ B_j = \begin{bmatrix} 0_3 \\ I_3 \\ 0_3 \end{bmatrix}, \ H_j = \begin{bmatrix} \alpha_1/\epsilon I_3 \\ \alpha_2/\epsilon^2 I_3 \\ \alpha_3/\epsilon^3 I_3 \end{bmatrix}, \\ C_j &= \begin{bmatrix} I_3 & 0_3 & 0_3 \end{bmatrix}, \ \text{for } j \in \{1, 2\}, \\ \bar{f}(\hat{\chi}^{(i)}, \theta_1, \dot{\bar{\theta}}_r^{(i_t)}) &= \begin{bmatrix} ge_z - \ddot{p}_r \\ f(\hat{\xi}^{(i)}, \theta_1, \dot{\bar{\theta}}_r^{(i_t)}) \end{bmatrix}, \\ \bar{G}^{(i)}(\theta_1) &= \begin{bmatrix} \frac{-R_3(\theta_1)}{m} & 0_3 \\ 0_{3\times 1} & G(\theta_1) \end{bmatrix} M \mathcal{BF}^{(i)}, \end{split}$$

where  $\oplus$  denotes the matrix direct sum, H is designed by choosing  $\alpha_1, \alpha_2, \alpha_3 \in \mathbb{R}_{>0}$  such that the polynomial

$$s^3 + \alpha_1 s^2 + \alpha_2 s + \alpha_3, \tag{9}$$

is Hurwitz [21] and  $\epsilon \in \mathbb{R}_{>0}$  is a tuning parameter that must be chosen small enough. In practice,  $\epsilon$  is tuned empirically to achieve a balance between convergence rate of the observer and noise amplification. All EHGO estimates must also be saturated outside a compact set of interest to avoid peaking, see *Remark 1* in [20].

## B. Output Feedback Control

The output feedback controllers are written using the estimates from the corresponding EHGO,  $\hat{\chi}^{(i)}$ . The family of translational output feedback controllers, induced by rotational reference signals and total thrust, become

$$\hat{\phi}_r^{(i)} = \tan^{-1} \left( \frac{-\hat{f}_y^{(i)}}{\sqrt{(\hat{f}_x^{(i)})^2 + (\hat{f}_z^{(i)} - g)^2}} \right), \quad \hat{\psi}_r^{(i)} = 0,$$

$$\hat{\theta}_r^{(i)} = \tan^{-1} \left( \frac{\hat{f}_x^{(i)}}{\hat{f}_z^{(i)} - g} \right), \quad \hat{u}_{fd}^{(i)} = -\frac{m(\hat{f}_z^{(i)} - g)}{\cos \hat{\phi}_r^{(i)} \cos \hat{\theta}_r^{(i)}},$$

where  $\hat{f}_t^{(i)} = [\hat{f}_x^{(i)} \ \hat{f}_y^{(i)} \ \hat{f}_z^{(i)}]^{\top} = -\gamma_1 \hat{\rho}_1^{(i)} - \gamma_2 \hat{\rho}_2^{(i)} - \hat{\sigma}_{\rho}^{(i)} + \ddot{p}_r$ . Here, desired heading,  $\hat{\psi}_r^{(i)}$ , is set to zero to simplify the control equations; see [22] for control equations with arbitrary  $\hat{\psi}_r^{(i)}$ . The family of rotational output feedback controllers become

$$\hat{\tau}_d^{(i)} = G^{-1}(\theta_1) \left[ \hat{f}_r^{(i)} - f(\hat{\xi}^{(i)}, \theta_1, \dot{\bar{\theta}}_r^{(i_t)}) \right],$$

where  $\hat{\boldsymbol{f}}_r^{(i)} = -\beta_1 \hat{\boldsymbol{\xi}}_1^{(i)} - \beta_2 \hat{\boldsymbol{\xi}}_2^{(i)} - \hat{\boldsymbol{\varsigma}}_{\boldsymbol{\xi}}^{(i)}$ . Note that the rotational reference signal estimates  $(\hat{\phi}_r^{(i_t)}, \hat{\theta}_r^{(i_t)}, \hat{\psi}_r^{(i_t)})$  are used to estimate  $\dot{\boldsymbol{\theta}}_r^{(i_t)}$  in  $\hat{\boldsymbol{\tau}}_d^{(i)}$  (see [20] for details). We then arrive at the family of commanded squared rotor speeds

$$\boldsymbol{\omega}_{s}^{(i)} = (M\mathcal{B}\mathcal{F}^{(i)})^{\dagger} \hat{\boldsymbol{u}}^{(i)}, \quad \hat{\boldsymbol{u}}^{(i)} = \begin{bmatrix} \hat{u}_{fd}^{(i)} \\ \hat{\tau}_{d}^{(i)} \\ \hat{\tau}_{d}^{(i)} \end{bmatrix}, \tag{10}$$

where  $(\cdot)^{\dagger} = (\cdot)^{\top} ((\cdot)(\cdot)^{\top})^{-1}$  is the minimum energy pseudo-inverse of the argument.

The rotational closed-loop system under input  $\omega_s^{(i_t)}$  for any  $i_t$ , regardless of  $i_t^*$ , reduces to the following perturbed linear system, since the mismatch is captured by  $\bar{\varsigma}_{\varepsilon}^{(i)}$ 

$$\dot{\boldsymbol{\xi}} = A_{\boldsymbol{\xi}} \boldsymbol{\xi} + \epsilon B_1 \boldsymbol{\delta}^{(i)}, \ A_{\boldsymbol{\xi}} = \begin{bmatrix} 0_3 & I_3 \\ -\beta_1 I_3 & -\beta_2 I_3 \end{bmatrix}, \ B_1 = \begin{bmatrix} 0_3 \\ I_3 \end{bmatrix}, \quad (11)$$

where

$$\epsilon \boldsymbol{\delta}^{(i)} = \boldsymbol{\varsigma}_{\xi} + \sigma_{m}^{(i)} - \hat{\boldsymbol{\varsigma}}_{\xi}^{(i)} + \beta_{1}(\boldsymbol{\xi}_{1} - \hat{\boldsymbol{\xi}}_{1}^{(i)}) + \beta_{2}(\boldsymbol{\xi}_{2} - \hat{\boldsymbol{\xi}}_{2}^{(i)}) + \Delta f^{(i)}, \quad \Delta f^{(i)} = f(\boldsymbol{\xi}, \boldsymbol{\theta}_{1}, \dot{\boldsymbol{\theta}}_{r}^{(i_{t})}) - f(\hat{\boldsymbol{\xi}}^{(i)}, \boldsymbol{\theta}_{1}, \dot{\boldsymbol{\theta}}_{r}^{(i_{t})}).$$
(12)

The ability to write the mismatched closed-loop system as (11) means that if  $\epsilon$  is chosen small enough, the system under output feedback will recover performance of the desired linear system, even in the presence of an actuator failure without requiring a model switch.

Remark 2 (Multiple Possible Recovery Strategies): For the small constants,  $\epsilon_1, \epsilon_2 \in \mathbb{R}_{>0}$ , where  $\epsilon_1 \ll \epsilon_2$ , if we choose  $\epsilon \in (0, \epsilon_1)$  a recovery can be achieved without requiring a model switch. If we choose  $\epsilon \in (\epsilon_1, \epsilon_2)$ , nominal disturbances can be compensated, however, the large disturbance,  $\sigma_m^{(i)}$ , can result in large estimation error. Due to practical constraints on  $\epsilon$  when it comes to implementation, such as sample rate and noise, we must choose  $\epsilon \in (\epsilon_1, \epsilon_2)$ . This motivates our use of multiple models and multiple observers for recovery (see *Theorem 1* for details). Furthermore, we can arrive at approximate values of  $\epsilon_1 \approx 0.002$  and  $\epsilon_2 \approx 0.06$  through simulation.

Remark 3 (Domain of Operation): We define the domain of operation as the region in which singularities are avoided in the feedback linearizing control design [20]. Since  $\sigma_m^{(i)} = 0$  for  $i = i_t^*$ , for any single actuator failure, with  $\epsilon \in (0, \epsilon_2)$  and  $i_t = i_t^*$ , the closed-loop rotational subsystem becomes the linearized system (11) with a small perturbation  $\epsilon \delta^{(i)}$ . Therefore, the domain of operation is the same for all  $i_t = i_t^*$ .

# IV. FAILURE RECOVERY STRATEGY

The most common external disturbances experienced by a multi-rotor during flight are aerodynamic (wind gusts, drag, etc.), and therefore primarily affect the translational dynamics. During an actuator failure, a large rotational torque is generated. This large torque appears as a high magnitude disturbance,  $\sigma_m^{(i)}$ , in the rotational dynamics, thus we monitor the rotational subsystem for actuator failure detection.

For  $\epsilon \in (\epsilon_1, \epsilon_2)$ , when  $i_t \neq i_t^*$  immediately after failure, the perturbation,  $\epsilon \delta^{(i_t)}$ , is no longer small, and may make (11) leave the domain of operation. This behavior can be identified by monitoring an estimate of the derivative of a Lyapunov function for the rotational subsystem, using the method presented in [23]. Therefore we can detect the failure, and then switch models to recover stability. Defining  $t_s$  as the time of control switching, we can define a maximum switching time,  $t_{s_{\text{max}}}$ , such that  $t_s < t_{s_{\text{max}}}$  ensures recovery from the failure before (11) leaves the domain of operation (see the proof of *Theorem 1* for an estimate of  $t_{s_{\text{max}}}$ ).

## A. Estimating the Lyapunov Derivative

Since the derivative of the Lyapunov function is not available, it will be estimated using estimates from the EHGOs, similar to [23]. Following Assumption 2, the system begins in the nominal operating regime,  $i_t^* = 0$ , therefore only the nominal Lyapunov function derivative must be estimated

$$\dot{\hat{V}}_{\xi} = \hat{\boldsymbol{\xi}}^{(0)\top} P_{\xi} \dot{\hat{\boldsymbol{\xi}}}^{(0)} + \dot{\hat{\boldsymbol{\xi}}}^{(0)\top} P_{\xi} \hat{\boldsymbol{\xi}}^{(0)}, \tag{13}$$

where  $P_{\xi}A_{\xi} + A_{\xi}^{T}P_{\xi} = -I_{6}$ . We use this estimate to test the following inequality to detect an actuator failure

$$\dot{\hat{V}}_{\xi} \le a_0 - \|\hat{\boldsymbol{\xi}}^{(0)}\|^2,\tag{14}$$

where  $a_0 \in \mathbb{R}_{>0}$  is a small constant introduced to overcome the  $O(\epsilon)$  estimation errors and is tuned empirically through simulation and experiments. For example, choosing  $a_0$  too small would result in detecting false positives, and too large would increase time until failure detection, potentially past  $t_{s_{\max}}$ . Once (14) is violated, a new model must be selected.

## B. Estimating Disturbance and Failures Simultaneously

Since all disturbance estimates contain any discrepancies between the modeled response and the response of the physical system, the total rotational disturbance estimated by the *i*-th observer,  $\hat{\boldsymbol{\varsigma}}_{\xi}^{(i)}$ , is an estimate of  $\boldsymbol{\sigma}_{m}^{(i)} + \boldsymbol{\varsigma}_{\xi}$ . In order to select the appropriate model after a failure has been detected using (14), we utilize the magnitude of the disturbance estimates from each observer to appropriately select  $i_{t} = i_{t}^{*}$  as

$$i_t = \arg\min_{i \in \{1, \dots, 6\}} \left\{ \left\| \hat{\bar{\varsigma}}_{\xi}^{(i)} \right\| \right\}.$$
 (15)

Following Assumption 2, (15) is a minimization across failure modes, excluding the nominal model.

## V. STABILITY ANALYSIS

Following the stability arguments in [20] and the theoretical analysis therein, the proposed output feedback control design presented here meets the same stability guarantees. We can show that these stability guarantees are also met under actuator failure without switching models when  $\epsilon \in (0, \epsilon_1)$ , and also hold for  $\epsilon \in (\epsilon_1, \epsilon_2)$  so long as  $i_t = i_t^*$ .

We must now investigate the stability of the system during an actuator failure. Define the scaled observer error for the rotational system,  $\boldsymbol{\eta}^{(i)} = [\boldsymbol{\eta}_1^{(i)} \ \boldsymbol{\eta}_2^{(i)} \ \boldsymbol{\eta}_3^{(i)}]^{\top} \in \mathbb{R}^9$ , by

$$\boldsymbol{\eta}_{1}^{(i)} = \frac{\boldsymbol{\xi}_{1} - \hat{\boldsymbol{\xi}}_{1}^{(i)}}{\epsilon^{2}}, \quad \boldsymbol{\eta}_{2}^{(i)} = \frac{\boldsymbol{\xi}_{2} - \hat{\boldsymbol{\xi}}_{2}^{(i)}}{\epsilon}, \quad \boldsymbol{\eta}_{3}^{(i)} = \boldsymbol{\varsigma}_{\xi} + \boldsymbol{\sigma}_{m}^{(i)} - \hat{\boldsymbol{\varsigma}}_{\xi}^{(i)}.$$

The entire rotational output feedback closed-loop system can now be written as the singularly perturbed system

$$\dot{\boldsymbol{\xi}} = A_{\mathcal{E}}\boldsymbol{\xi} + \epsilon B_1 \boldsymbol{\delta}^{(i)},\tag{16a}$$

$$\epsilon \dot{\boldsymbol{\eta}}^{(i)} = \Lambda \boldsymbol{\eta}^{(i)} + \epsilon \left( B_2 \frac{\Delta f^{(i)}}{\epsilon} + B_3 (\varphi_{\mathcal{E}}^{(i)}(t, \boldsymbol{\bar{\varsigma}}_{\mathcal{E}}^{(i)}) + \dot{\boldsymbol{\sigma}}_m^{(i)}) \right), \tag{16b}$$

where the system dynamics (16a) are the slow variables, the observer error (16b) are the fast variables, and

$$\Lambda = \begin{bmatrix} -\alpha_1 I_3 & I_3 & 0_3 \\ -\alpha_2 I_3 & 0_3 & I_3 \\ -\alpha_3 I_3 & 0_3 & 0_3 \end{bmatrix}, \quad B_2 = \begin{bmatrix} 0_3 \\ I_3 \\ 0_3 \end{bmatrix}, \quad B_3 = \begin{bmatrix} 0_3 \\ 0_3 \\ I_3 \end{bmatrix}.$$

By Assumption 3,  $\varphi_{\xi}^{(i)}(t, \bar{\varsigma}_{\xi}^{(i)})$  is continuous and bounded, and it can be shown that  $\dot{\sigma}_{m}^{(i)}$  is also continuous and bounded, so we can bound the sum as,  $\varphi_{\xi}^{(i)}(t, \bar{\varsigma}_{\xi}^{(i)}) + \dot{\sigma}_{m}^{(i)} \leq \Delta_{\max}^{(i)}$ .

From [20],  $\Delta f^{(i)}$  is Lipschitz in  $\xi$  over the domain of operation and  $\Delta f^{(i)}$  can be bounded by  $\|\Delta f^{(i)}\| \le \epsilon L_{\eta} \|\eta^{(i)}\|$ , for the Lipschitz constant,  $L_{\eta}$ . We can write a Lyapunov function for the scaled observer error system (16b) as

$$V_{\eta}^{(i)} = (\boldsymbol{\eta}^{(i)})^{\mathsf{T}} P_{\eta} \boldsymbol{\eta}^{(i)}, \quad \text{where } P_{\eta} \Lambda + \Lambda^{\mathsf{T}} P_{\eta} = -I_{9}. \tag{17}$$

Lemma 1 (Bounds on Observer Error): Let the observer error at the time of failure,  $t_f$ , be  $\eta^{(i)}(t_f)$ . Then, the observer error for  $t > t_f$  can be bounded by

$$\begin{split} \left\| \boldsymbol{\eta}^{(i)}(t) \right\| & \leq \left( \left( \sqrt{V_{\eta}^{(i)}(t_f)} - \epsilon \frac{\kappa}{c} \right) e^{-\frac{c(t - t_f)}{\epsilon}} + \epsilon \frac{\kappa}{c} \right) / \sqrt{\lambda_{\min}(P_{\eta})}, \\ c & = \left( \frac{1}{\lambda_{\max}(P_{\eta})} - \frac{\lambda_{\max}(P_{\eta}) \epsilon L_{\eta}}{\lambda_{\min}(P_{\eta})} \right), \quad \kappa = \frac{\lambda_{\max}(P_{\eta}) \Delta_{\max}^{(i)}}{\sqrt{\lambda_{\min}(P_{\eta})}}, \end{split}$$

where  $\lambda_{\min}(\cdot)$  and  $\lambda_{\max}(\cdot)$  are the minimum and maximum eigenvalues of the argument, respectively.

*Proof:* Taking the Lyapunov function (17) and computing the derivative with the scaled observer error system (16b) yields

$$\begin{split} \epsilon \dot{V}_{\eta}^{(i)} &= -(\boldsymbol{\eta}^{(i)})^{\top} \boldsymbol{\eta}^{(i)} \\ &+ 2 \epsilon (\boldsymbol{\eta}^{(i)})^{\top} P_{\eta} \left( B_2 \frac{\Delta f^{(i)}}{\epsilon} + B_3 (\varphi_{\varepsilon}^{(i)}(t, \boldsymbol{\bar{\varsigma}}_{\varepsilon}^{(i)}) + \dot{\sigma}_m^{(i)}) \right), \end{split}$$

which can be bounded by

$$\begin{split} \epsilon \dot{V}_{\eta}^{(i)} &\leq -\frac{c}{2} V_{\eta}^{(i)} + 2\epsilon \kappa \sqrt{V_{\eta}^{(i)}}, \\ c &= \left(\frac{1}{\lambda_{\max}(P_{\eta})} - \frac{\lambda_{\max}(P_{\eta})\epsilon L_{\eta}}{\lambda_{\min}(P_{\eta})}\right), \quad \kappa = \frac{\lambda_{\max}(P_{\eta})\Delta_{\max}^{(i)}}{\sqrt{\lambda_{\min}(P_{\eta})}}. \end{split}$$

Taking  $W_{\eta}^{(i)} = \sqrt{V_{\eta}^{(i)}}$ , the bound becomes

$$\dot{W}_{\eta}^{(i)} \le -cW_{\eta}^{(i)} + \epsilon \kappa.$$

By the Comparison Lemma [24, *Lemma 3.4*],  $W_{\eta}^{(i)}(t)$  is upper bounded by

$$W_{\eta}^{(i)}(t) \leq \left(W_{\eta}^{(i)}(t_f) - \epsilon \frac{\kappa}{c}\right) e^{-\frac{c}{\epsilon}(t - t_f)} + \epsilon \frac{\kappa}{c},$$

leading to the bound on scaled observer error

$$\|\boldsymbol{\eta}^{(i)}(t)\| \le W_{\boldsymbol{\eta}}^{(i)}(t)/\sqrt{\lambda_{\min}(P_{\boldsymbol{\eta}})}.$$

We can now write (12) as

$$\epsilon \delta^{(i)} = \epsilon^2 \beta_1(\eta_1^{(i)}) + \epsilon \beta_2(\eta_2^{(i)}) + \eta_3^{(i)} + \Delta f^{(i)}, \quad (18)$$

which can be bounded in terms of observer error as

$$\epsilon \delta^{(i)} \le \delta_{\max}^{(i)}(t) = (\epsilon^2 \beta_1 + \epsilon(\beta_2 + L_{\eta}) + 1) \| \eta^{(i)}(t) \|.$$
 (19)

Lemma 1 shows that estimation error,  $\eta^{(i)}$ , converges to an  $O(\epsilon \Delta_{\max}^{(i)})$  neighborhood of the origin within  $O(\epsilon)$  time. Actuator failure is significantly more dynamic than external disturbance, i.e.,  $\dot{\boldsymbol{\varsigma}}_{\mathcal{E}}$  is relatively small as compared with  $\dot{\boldsymbol{\sigma}}_m^{(i)}$ . Thus,  $\Delta_{\max}^{(i_t^*)} \ll \Delta_{\max}^{(i)}$  for  $i \neq i_t^*$ , since  $\dot{\boldsymbol{\sigma}}_m^{(i_t^*)} = 0$ . Therefore, as stated in Remark 2,  $\epsilon$  can be chosen larger for the correct model than for any incorrect model, motivating the use of multiple models to reduce the total system disturbance.

In order to select the appropriate model after failure, as long as  $\sigma_m^{(i)}$ ,  $\varsigma_{\mathcal{E}}$ , and  $\|\eta_3^{(i)}(t_s)\|$  satisfy,

$$\|\sigma_m^{(i)}\| \ge 2\|\varsigma_{\mathcal{E}}\| + \|\eta_3^{(i)}(t_s)\| + \|\eta_3^{(i_t^*)}(t_s)\|,$$
 (20)

for each  $i \in \{1, ..., 6\} \setminus \{i_t^*\}$ , the observer estimate,  $\hat{\varsigma}^{(i_t^*)}$ , will be the smallest in magnitude at  $t_s$ , therefore, (15) will select the appropriate model.

Proposition 1 (Correct Model Selection): Under the control input,  $\omega_s^{(i_t)}$ , the family of observers (8) will produce disturbance estimates,  $\hat{\boldsymbol{\varsigma}}_{\xi}^{(i)}$ , for  $i \in \{0,\ldots,6\}$ . If  $\boldsymbol{\sigma}_m^{(i)}$ ,  $\boldsymbol{\varsigma}_{\xi}$ , and  $\|\boldsymbol{\eta}_3^{(i)}(t_s)\|$  satisfy (20), the estimate  $\hat{\boldsymbol{\varsigma}}_{\xi}^{(i_t^*)}$  will be the smallest in magnitude and (15) will select the correct model.

*Proof:* Suppose the modeling and external disturbances,  $\varsigma_{\xi}$ , the disturbance resulting from incorrect model selection,  $\sigma_m^{(i)}$ , and the scaled observer error,  $\|\eta_3^{(i)}(t_s)\|$  satisfy (20), then

$$\begin{split} \hat{\varsigma}_{\xi}^{(i)} &= \varsigma_{\xi} + \sigma_{m}^{(i)} - \eta_{3}^{(i)} \\ &\geq \|\sigma_{m}^{(i)}\| - (\|\varsigma_{\xi}\| + \|\eta_{3}^{(i)}\|) \\ &\geq \sup_{\text{using (20)}} (\|\varsigma_{\xi}\| + \|\eta_{3}^{(i_{t}^{*})}\|) \geq \varsigma_{\xi} - \eta_{3}^{(i_{t}^{*})} = \hat{\varsigma}_{\xi}^{(i_{t}^{*})}, \end{split}$$

where the last equality holds since  $\sigma_m^{(i_t^*)} = 0$ . Thus, the estimated disturbance,  $\hat{\mathbf{\varsigma}}_{\xi}^{(i_t^*)}$ , will be the smallest in magnitude at  $t_s$ , and the solution to (15) will be the correct model.

Remark 4 (Minimum Switching Time): At  $t_f$ ,  $\|\boldsymbol{\eta}_3^{(i)}(t_f)\|$  may be large, but will decay to an  $O(\epsilon \Delta_{\max}^{(i)})$  neighborhood of the origin in  $O(\epsilon)$  time. Therefore, there is some  $O(\epsilon)$  time we must wait to switch for the observer estimates to converge. Furthermore,  $\|\boldsymbol{\eta}_3^{(i_t^*)}(t)\|$  will decay to an  $O(\epsilon \Delta_{\max}^{(i_t^*)})$  neighborhood of the origin, further reducing  $\|\hat{\boldsymbol{\varsigma}}_{\xi}^{(i_t^*)}\|$  as compared with the other model estimates, since  $\Delta_{\max}^{(i_t^*)} \ll \Delta_{\max}^{(i)}$ .

Theorem 1 (Stability During Actuator Failure): Let the state of the system (11) at the time of failure,  $t_f$ , be such that  $V_{\xi}(t_f) < a$  for some sufficiently small a > 0. Then, there exist  $\epsilon_1, \epsilon_2 > 0$ , and maximum switching time,  $t_{s_{\max}} > t_f$ , such that the state,  $\xi$ , will remain within the domain of operation during the failure transient, and will recover tracking performance

- i) after the transient, when  $\epsilon \in (0, \epsilon_1)$ ;
- ii) if the correct model,  $i_t = i_t^*$ , is selected before  $t_{S_{\max}}$ , when  $\epsilon \in (\epsilon_1, \epsilon_2)$ .

*Proof:* A common Lyapunov function,  $V_{\xi}$ , for the feedback linearized rotational subsystem for each  $i \in \{0, ..., 6\}$  and  $\epsilon \to 0$  is given by

$$V_{\mathcal{E}} = \boldsymbol{\xi}^{\mathsf{T}} P_{\mathcal{E}} \boldsymbol{\xi}, \quad \text{where } P_{\mathcal{E}} A_{\mathcal{E}} + A_{\mathcal{E}}^{\mathsf{T}} P_{\mathcal{E}} = -I_6.$$
 (21)

Let  $\Omega_{\xi} = \{V_{\xi} < c_{\xi}\}$  be an estimate of the domain of operation of the controller designed in Section III-B for  $c_{\xi} \in \mathbb{R}_{>0}$  (see [20] for more details). For simplicity, we use the estimate of the domain of operation for  $\epsilon \to 0$ , wherein the states and disturbances are estimated perfectly. For small  $\epsilon > 0$ , the obtained domain of operation can be shrunk to  $\Omega'_{\xi} = \{V_{\xi} < c'_{\xi}\}$ , with  $c'_{\xi} < c_{\xi}$ , to incorporate the effect of estimation error [25].

Using arguments similar to singular perturbation [24, *Theorem 11.4*] and non-vanishing perturbation [24, *Lemma 9.2*], it can be shown that (16) converges to an  $O(\epsilon \Delta_{\max}^{(i)})$  neighborhood of the origin for  $\epsilon \in (0, \epsilon_2)$ . For  $\epsilon \in (0, \epsilon_1)$  the neighborhood  $O(\epsilon \Delta_{\max}^{(i)})$  is small enough for reasonable tracking performance. For  $\epsilon \in (\epsilon_1, \epsilon_2)$ , the large estimation error can make the trajectory leave the domain of operation and the system may diverge, thus requiring a model switch.

Taking the Lyapunov function (21), and computing its derivative with the rotational closed-loop system (11) yields

$$\dot{V}_{\xi} = -\boldsymbol{\xi}^{\mathsf{T}}\boldsymbol{\xi} + 2\boldsymbol{\xi}^{\mathsf{T}}P_{\xi}\epsilon B_{1}\boldsymbol{\delta}^{(i)}.$$
 (22)

By the change of variables  $W_{\xi} = \sqrt{V_{\xi}}$ , and the arguments in the proof of *Lemma 1*, we can immediately upper bound  $W_{\xi}(t)$  by

$$W_{\xi}(t_f)e^{\frac{-(t-t_f)}{2\lambda_{\max}(P_{\xi})}} + \int_{t_f}^t e^{\frac{-(t-\tau)}{2\lambda_{\max}(P_{\xi})}} \frac{\lambda_{\max}(P_{\xi})}{\sqrt{\lambda_{\min}(P_{\xi})}} \delta_{\max}^{(i)}(\tau) d\tau.$$

Let  $t = t_{s_{\text{max}}}$  be the unique solution to the equation

$$\sqrt{a}e^{\frac{-(t-t_f)}{2\lambda_{\max}(P_\xi)}} + \int_{t_f}^t e^{\frac{-(t-\tau)}{2\lambda_{\max}(P_\xi)}} \frac{\lambda_{\max}(P_\xi)}{\sqrt{\lambda_{\min}(P_\varepsilon)}} \delta_{\max}^{(i)}(\tau) d\tau = c_\xi.$$

The theorem follows immediately from the definition of  $t_{S_{\text{max}}}$ .

## VI. SIMULATION

The proposed method is simulated for a hexrotor system tracking a trajectory generated by a 9-th order polynomial to ensure sufficient smoothness, shown in Fig. 2. The system is simulated in discrete-time with sample time, T=0.01s, while using position and orientation measurements with added white Gaussian noise to replicate the experimental system. The hexrotor is able to track the reference trajectory, suffer an actuator failure at 14 seconds into flight, and recover to resume tracking the trajectory after switching controllers. The system is simulated with large external rotational disturbances,  $\sigma_{\xi} = 12[\sin(t) \cos(t) \sin(t)]^{T}$ , and translational disturbances,  $\sigma_{\Omega} = [\sin(t) \cos(t) \sin(t)]^{T}$ .

To facilitate tuning the parameters, for example  $\epsilon$ ,  $a_0$ , and control gains, we use the same parameters in simulation as in the experiment. The parameters are given in Table I,

 $\label{table I} \textbf{TABLE I}$  System parameters used in simulation and experiment.

$\epsilon$	$b^+$	r	c	<b>γ</b> 1	$\beta_1$	$\alpha_1$	$\alpha_3$
0.025	1.8182e-5	0.275m	0.1	2	40	3	0.6
	1 -		1				
$\tau_m$	$b^-$	m	$a_0$	$\gamma_2$	$\beta_2$	$\alpha_2$	T

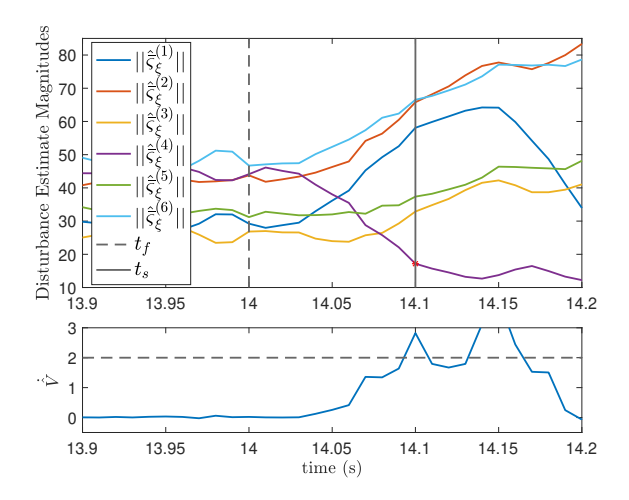


Fig. 1. Norm of disturbance estimates for all failure case models and Lyapunov derivative estimate during a simulated in-flight actuator failure.

and the inertia matrix J is a diagonal matrix with entries  $\{0.0228, 0.0241, 0.0446\}$  kg m<sup>2</sup>.

The estimated Lyapunov function derivative,  $\hat{V}_{\xi}$ , is monitored to determine when the failure occurs. The magnitudes of the estimated disturbances for all six failure modes, as well as the Lyapunov derivative estimate, are shown in Fig. 1. At the time of detection,  $\hat{\varsigma}_{\xi}^{(4)}$  has the smallest magnitude, indicating a failure of actuator four. The dashed vertical line in Fig. 1 shows the time when a failure is induced,  $t_f$ , and the solid vertical line shows when the switch occurs,  $t_s$ .

Fig. 2 shows the hexrotor briefly breaking from tracking the reference trajectory as the failure occurs at  $t_f$ , and after

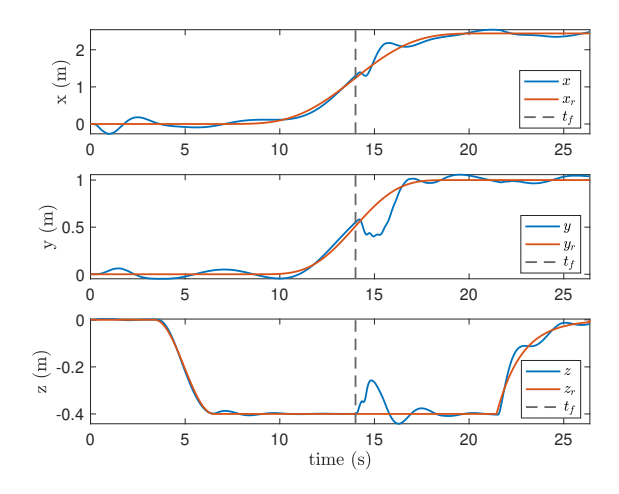


Fig. 2. Hexrotor position tracking recovery after simulated in-flight actuator failure using multiple models to recover performance.

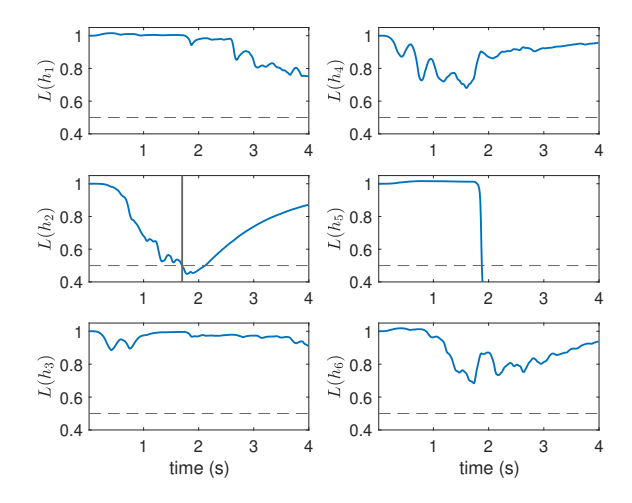


Fig. 3. Health estimate of each rotor as estimated using the Extended Kalman Filter method.

the controller is switched, the hexrotor successfully resumes tracking the trajectory. The tracking performance is slightly degraded due to the large external disturbances present in this simulation, however, a successful recovery is still achieved.

A potential problem with not considering disturbance is the false identification of failures. We illustrate this with the rotor health estimation approach [11]. This method utilizes an Extended Kalman Filter which estimates the health of each rotor,  $h_i$ , for  $j \in \{1, ..., 6\}$ . Utilizing the same dynamics and a detection cutoff on the health of each rotor of 0.5, as was shown to work well experimentally in [11], we simulate this method. The same flight parameters and large disturbances are again applied to the system with the EHGO based failure detection method replaced by the EKF method. The EKF method does not consider disturbances, and Fig. 3 shows that a failure of actuator two is falsely detected just under two seconds into flight. In principle, the EKF could be augmented with a disturbance model to improve this performance, however, that would require a model of the expected disturbances [19]. The EHGO can accommodate a wide range of disturbances with unknown dynamics. We also investigated lowering the health cutoff threshold below 0.5. however, this results in longer detection times. In summary, depending on flight conditions, considering disturbance in the failure recovery strategy becomes important.

# VII. EXPERIMENTAL VALIDATION

The proposed multiple-model estimation and control method is implemented on an experimental platform to validate performance and show recovery from an actuator failure during flight. The experimental platform is built on a 550mm hexrotor frame with 920kV motors and 10x4.5 carbon fiber rotors. Six 35A ESCs with bidirectional capability are used, and the system is powered by a 5000mAh 4s LiPo battery.

The control method is implemented on a Pixhawk 4 FMU in discrete time at 100Hz using Mathworks Simulink through the *PX4 Autopilots Support from Embedded Coder* package. All sensing and computation is done on-board the vehicle, with

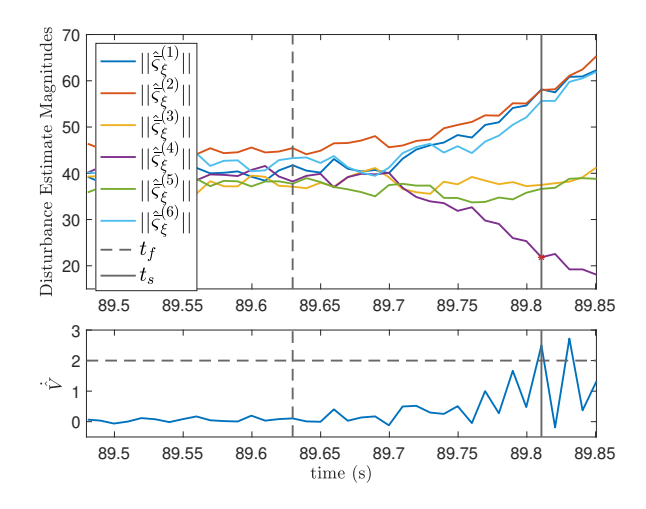


Fig. 4. Norm of disturbance estimates for all failure case models and Lyapunov derivative estimate during an experimental in-flight actuator failure.

the exception of utilizing translational position data from a Vicon motion capture system in lieu of GPS.

Once the failure is detected and the controller is switched, the rotor opposite the failed rotor will be commanded to reverse directions to apply a large downward force to counteract the roll and pitch errors. Once the system returns to level flight, using the pseudo-inverse to compute desired rotor speeds results in the opposite rotor being commanded to apply small forces in either direction, thus requiring the rotor to change directions rapidly. During experimental testing it became clear that the opposite rotor could not change directions quickly enough to stabilize the system. To restrict the opposite rotor to only generate downward force for a detected failure, i, we impose force constraints,  $f_{\min}^{(i,j)}$ ,  $f_{\max}^{(i,j)}$  < 0 for the opposite rotor, j, defined by

$$j = \begin{cases} i+3, & 1 \le i \le 3, \\ i-3, & 4 \le i \le 6, \end{cases}$$

and  $f_{\min}^{(i,j)}, f_{\max}^{(i,j)} \geq 0$  for all remaining j. These constraints ensure only a single directional change will be commanded when the model is switched. Let  $\bar{f}^*$  be the solution to the following optimization problem with above discussed constraints under the selected model  $i_t$ 

$$\begin{split} & \underset{\bar{f}}{\text{minimize}} & \left( \left\| \bar{f} \right\|^2 + \lambda \left\| W_{\nu} \left( M \mathcal{F}^{(i_t)} \bar{f} - \hat{\boldsymbol{u}}^{(i_t)} \right) \right\|^2 \right) \\ & \text{subject to} & f_{\min}^{(i,j)} \leq \bar{f}_{i,j}^* \leq f_{\max}^{(i,j)}, \end{split}$$

where  $\lambda \in \mathbb{R}_{>0}$  is chosen to be large to ensure we achieve applied forces and torques as close as possible to the desired  $\hat{\boldsymbol{u}}^{(i_t)}$ . We also take advantage of the diagonal weighting matrix,  $W_v \in \mathbb{R}^{4\times 4}$ , to prioritize the total thrust and the roll and pitch torques, allowing for lower performance in yaw tracking since the former are integral for achieving a successful recovery. The additional  $\|\bar{\boldsymbol{f}}\|^2$  term is used to simultaneously select a solution with lower energy. The solution,  $\bar{\boldsymbol{f}}^*$ , is then mapped to squared rotor speeds through the inverse of (3). The optimization problem is solved by the active-set algorithm proposed in [26].

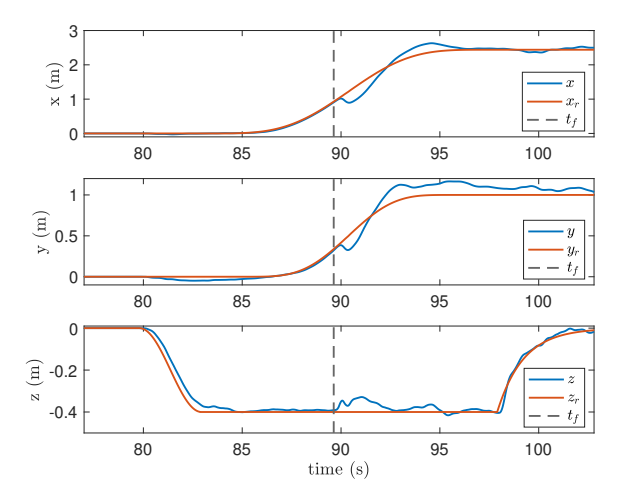


Fig. 5. Hexrotor position tracking recovery after experimental in-flight actuator failure.

The experimental system is flown along the same trajectory as in simulation and a failure of actuator four is induced algorithmically. The norm of the experimental disturbance estimates for each failure model, and the Lyapunov derivative estimate, are shown in Fig. 4. The dashed vertical line in Fig. 4 corresponds to the time when a failure is induced,  $t_f$ , and the solid vertical line shows when the detection and switch occurs,  $t_s$ . The correct model for a failure of actuator four is selected and the resulting tracking performance before and after recovery are shown in Fig. 5. The tracking performance after failure is slightly degraded due to the use of non-ideal control inputs,  $\bar{f}^*$ . A video of the experiments can be found at https://youtu.be/8fQMrca49os

# VIII. CONCLUSIONS AND FUTURE WORK

We studied a trajectory tracking problem for a hexrotor in the presence of modeling error and external disturbances, while simultaneously enabling in-flight recovery of a complete actuator failure. A multiple-model, multiple EHGO based output feedback control framework is used to enable this extended functionality. The framework is rigorously analyzed to provide stability guarantees and bounds on the maximum switching time for recovery. Simulation and experimental flight data show the successful application of the method on a physical system.

Future work includes the extension to multiple failures for general *n*-rotors. Assuming that system controllability is retained despite multiple failures, the proposed approach could be applied in an hierarchical way, wherein a new set of models are considered after each failure detection. Analysis of such an approach under mutual interactions of multiple failures is an interesting direction of future investigation.

## IX. ACKNOWLEDGEMENTS

We would like to thank Professor Hassan K. Khalil for his insights on extended high-gain observer design and analysis.

#### REFERENCES

- I. Hwang, S. Kim, Y. Kim, and C. E. Seah, "A survey of fault detection, isolation, and reconfiguration methods," *IEEE Transactions on Control Systems Technology*, vol. 18, no. 3, pp. 636–653, 2009.
- [2] J. D. Boskovic, S.-H. Yu, and R. K. Mehra, "A stable scheme for automatic control reconfiguration in the presence of actuator failures," in *Proceedings of American Control Conference*. IEEE, 1998, pp. 2455– 2459.

- [3] J. D. Boskovic and R. K. Mehra, "Stable multiple model adaptive flight control for accommodation of a large class of control effector failures," in *Proceedings of American Control Conference*. IEEE, 1999, pp. 1920– 1924
- [4] A. Chakravarty, T. K. Nizami, I. Kar, and C. Mahanta, "Adaptive compensation of actuator failures using multiple models," *IFAC World Congress*, vol. 50, no. 1, pp. 10350–10356, 2017.
- [5] M. W. Mueller and R. D'Andrea, "Stability and control of a quadro-copter despite the complete loss of one, two, or three propellers," in *International Conference on Robotics and Automation (ICRA)*. IEEE, 2014, pp. 45–52.
- [6] D. Xu, J. F. Whidborne, and A. Cooke, "Fault tolerant control of a quadrotor using L₁ adaptive control," *International Journal of Intelli*gent Unmanned Systems, vol. 4, no. 1, pp. 43–66, 2016.
- [7] T. Avant, U. Lee, B. Katona, and K. Morgansen, "Dynamics, hover configurations, and rotor failure restabilization of a morphing quadrotor," in *American Control Conference (ACC)*. IEEE, 2018, pp. 4855–4862.
- [8] Z. T. Dydek, A. M. Annaswamy, and E. Lavretsky, "Adaptive control of quadrotor UAVs: A design trade study with flight evaluations," *IEEE Transactions on Control Systems Technology*, vol. 21, no. 4, pp. 1400– 1406, 2012.
- [9] P. Lu and E.-J. van Kampen, "Active fault-tolerant control for quadrotors subjected to a complete rotor failure," in *International Conference on Intelligent Robots and Systems (IROS)*. IEEE, 2015, pp. 4698–4703.
- [10] D. Vey and J. Lunze, "Structural reconfigurability analysis of multirotor UAVs after actuator failures," in *Conference on Decision and Control*. IEEE, 2015, pp. 5097–5104.
- [11] D. Tzoumanikas, Q. Yan, and S. Leutenegger, "Nonlinear MPC with motor failure identification and recovery for safe and aggressive multicopter flight," in *International Conference on Robotics and Automation* (ICRA). IEEE, 2020, pp. 8538–8544.
- [12] D. Vey and J. Lunze, "Experimental evaluation of an active fault-tolerant control scheme for multirotor UAVs," in *Conference on Control and Fault-Tolerant Systems (SysTol)*. IEEE, 2016, pp. 125–132.
- [13] R. Voyles and G. Jiang, "Hexrotor UAV platform enabling dextrous interaction with structures—Preliminary work," in *International Symposium* on Safety, Security, and Rescue Robotics (SSRR). IEEE, 2012, pp. 1–7.
- [14] H. Alwi and C. Edwards, "Fault tolerant control of octorotor using sliding mode control allocation," in *Proceedings of the EuroGNC Specialist Conference on Guidance, Navigation & Control*, 2013, pp. 1404–1423.
- [15] —, "Sliding mode fault-tolerant control of an octorotor using linear parameter varying-based schemes," *IET Control Theory & Applications*, vol. 9, no. 4, pp. 618–636, 2015.
- [16] G. Michieletto, M. Ryll, and A. Franchi, "Fundamental actuation properties of multirotors: Force-moment decoupling and fail-safe robustness," *Transactions on Robotics*, vol. 34, no. 3, pp. 702–715, 2018.
- [17] M. Kamel, T. Stastny, K. Alexis, and R. Siegwart, "Model predictive control for trajectory tracking of unmanned aerial vehicles using robot operating system," in *Robot Operating System (ROS)*. Springer, 2017, pp. 3–39.
- [18] D. Hentzen, T. Stastny, R. Siegwart, and R. Brockers, "Disturbance estimation and rejection for high-precision multirotor position control," in *IEEE/RSJ International Conference on Intelligent Robots and Systems* (IROS), 2019, pp. 2797–2804.
- [19] A. Radke and Z. Gao, "A survey of state and disturbance observers for practitioners," in *American Control Conference*. IEEE, 2006, pp. 6–pp.
   [20] C. J. Boss, V. Srivastava, and H. K. Khalil, "Robust tracking of an
- [20] C. J. Boss, V. Srivastava, and H. K. Khalil, "Robust tracking of an unknown trajectory with a multi-rotor UAV: A high-gain observer approach," in *American Control Conference*, Denver, CO, Jul. 2020, pp. 1429–1434.
- [21] H. K. Khalil, High-Gain Observers in Nonlinear Feedback Control. Philadelphia, PA, USA: SIAM, 2017.
- [22] C. J. Boss, J. Lee, and J. Choi, "Uncertainty and disturbance estimation for quadrotor control using extended high-gain observers: Experimental implementation," in ASME Dynamic Systems and Control Conference, 2017, p. V002T01A003.
- [23] L. B. Freidovich and H. K. Khalil, "Lyapunov-based switching control of nonlinear systems using high-gain observers," *Automatica*, vol. 43, no. 1, pp. 150–157, 2007.
- [24] H. K. Khalil, Nonlinear Systems. Upper Saddle River, 2002.
- [25] C. J. Boss and V. Srivastava, "A high-gain observer approach to robust trajectory estimation and tracking for a multi-rotor UAV," arXiv preprint arXiv:2103.13429, 2021.
- [26] O. Harkegard, "Efficient active set algorithms for solving constrained least squares problems in aircraft control allocation," in *IEEE Conference* on Decision and Control, 2002, pp. 1295–1300.